Molecular Microbiology (2009) 73(4), 710–718 ■
doi:10.1111/j.1365-2958.2009.06802.x
First published online 27 July 2009

Stator assembly and activation mechanism of the flagellar motor by the periplasmic region of MotB

Seiji Kojima,[1,2†] Katsumi Imada,[2,3*†] Mayuko Sakuma,[1] Yuki Sudo,[1] Chojiro Kojima,[4] Tohru Minamino,[2,3] Michio Homma[1] and Keiichi Namba[2,3***]**

[1]*Division of Biological Science, Graduate School of Science, Nagoya University, Furo-Cho, Chikusa-Ku, Nagoya 464-8602, Japan.*
[2]*Dynamic NanoMachine Project, ICORP, JST, 1-3 Yamadaoka, Suita, Osaka 565-0871, Japan.*
[3]*Graduate School of Frontier Biosciences, Osaka University, 1-3 Yamadaoka, Suita, Osaka 565-0871, Japan.*
[4]*Laboratory of Biophysics, Graduate School of Biological Sciences, Nara Institute of Science and Technology (NAIST), 8916-5 Takayama, Ikoma, Nara 630-0192, Japan.*

Summary

Torque generation in the *Salmonella* flagellar motor is coupled to translocation of H^+ ions through the proton-conducting channel of the Mot protein stator complex. The Mot complex is believed to be anchored to the peptidoglycan (PG) layer by the putative peptidoglycan-binding (PGB) domain of MotB. Proton translocation is activated only when the stator is installed into the motor. We report the crystal structure of a C-terminal periplasmic fragment of MotB ($MotB_C$) that contains the PGB domain and includes the entire periplasmic region essential for motility. Structural and functional analyses indicate that the PGB domains must dimerize in order to form the proton-conducting channel. Drastic conformational changes in the N-terminal portion of $MotB_C$ are required both for PG binding and the proton channel activation.

Introduction

The bacterial flagellum is a long, filamentous organelle that extends out from the cell body and rotates to drive bacterial motility. The flagellum is made of three major parts: the basal body, the hook and the filament. The basal body works as a reversible rotary motor, and the filament, typically 10–15 μm long, serves as a helical propeller. The hook is a universal joint that connects the motor with the filament to transmit torque regardless of the orientation of the filament. The flagellar motor is a membrane-embedded nanomachine powered by the electrochemical potential difference of hydrogen or sodium ions across the cytoplasmic membrane (Manson *et al.*, 1977; Matsuura *et al.*, 1977; Hirota and Imae, 1983; as review articles, see Berg, 2003; Minamino *et al.*, 2008; Sowa and Berry, 2008; Terashima *et al.*, 2008). In the *Salmonella* and *Escherichia coli* motor, torque is generated by rotor–stator interactions coupled with proton translocation through the channel formed within the stator. The Mot complex is composed of two cytoplasmic membrane proteins, MotA and MotB, which form a $MotA_4$/$MotB_2$ hetero-hexameric complex (Terashima *et al.*, 2008). About a dozen stator complexes assemble around the rotor (Reid *et al.*, 2006) and are believed to anchor to the peptidoglycan (PG) layer (Chun and Parkinson, 1988; De Mot and Vanderleyden, 1994; Muramoto and Macnab, 1998). When the basal body is isolated by solubilizing cell membranes with detergents, the stator complex is lost from the basal body due to its transient interaction to the rotor. Therefore, structural information on the rotor–stator interaction is limited. No structural information is available for the isolated MotA/MotB complex, either. Therefore, our present understanding on the molecular mechanisms of torque generation and energy conversion is limited.

MotA has four transmembrane segments and a large cytoplasmic loop, which contains conserved charged residues that are thought to interact with those of a rotor protein, FliG (Zhou *et al.*, 1998a). MotB is composed of a small N-terminal cytoplasmic segment (residues 1–28), a single transmembrane helix (residues 29–50) and a large C-terminal periplasmic region (residues 51–309) (Muramoto and Macnab, 1998) (Fig. 1). The transmembrane helix, which contains a critical aspartate residue (Asp-33) required for proton translocation across the cell membrane, forms the proton channel together with two of the transmembrane segments of MotA (Blair and Berg, 1990; Stolz and Berg, 1991; Zhou *et al.*, 1998b; Che *et al.*, 2008). The periplasmic region of MotB contains a putative

Accepted 10 July, 2009. For correspondence. *E-mail kimada@fbs.osaka-u.ac.jp; Tel. (+81) 6 6879 4625; Fax (+81) 6 6879 4652; **E-mail g44416a@cc.nagoya-u.ac.jp; Tel. (+81) 52 789 2991; Fax (+81) 52 789 3001; or ***E-mail keiichi@fbs.osaka-u.ac.jp; Tel. (+81) 6 6879 4653; Fax (+81) 6 6879 4652. †These authors contributed equally to this work.

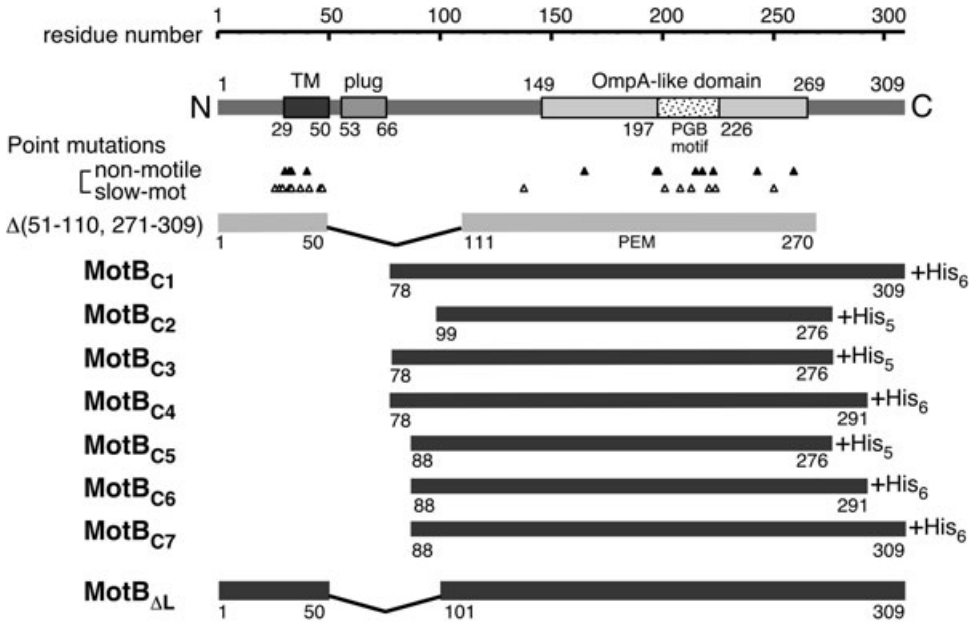

Fig. 1. Primary structure of MotB and schematic representation of $MotB_C$ variants used in this study. MotB contains 309 amino acids and has a single transmembrane domain ('TM', residues 30–50) in its N-terminal region. The large periplasmic region includes an 'OmpA-like domain' (residues 149–269) with a peptidoglycan-binding (PGB) motif (residues 197–226) that is well conserved among proteins such as OmpA, Pal and MotY. OmpA and Pal are known to bind to the peptidoglycan (PG) layer non-covalently. A segment that has been shown to act as a 'plug' of the proton channel to prevent premature proton translocation across the cell membrane is also shown ('plug', residues 53–66). Point mutations identified in previous studies (Blair *et al*., 1991; Togashi *et al*., 1997) and the smallest, functional protein [Δ(51–110, 271–309) (Muramoto and Macnab, 1998)] are shown below the primary structure. $MotB_C$ variants used for crystallization and a MotB deletion variant used for functional assay (Δ51–100, $MotB_{\Delta L}$) are shown in black bars.

peptidoglycan-binding (PGB) motif (De Mot and Vanderleyden, 1994), which is believed to anchor the MotA/MotB complex to the PG layer around the rotor. Residues 149–269 of MotB show sequence similarity to other OmpA-like proteins (UniProt Accession NO. P55892). Most amino acid substitutions in *motB* that impair motility are within or adjacent to the PGB motif or within the transmembrane helix. Thus, anchoring the MotA/MotB complex to the PG layer is essential for the motor function (Blair *et al*., 1991; Togashi *et al*., 1997). Since the PG layer is separated from the outer surface of the hydrophobic core layer of the cytoplasmic membrane by about 100 Å (Matias *et al*., 2003; A. Okada *et al*., pers. comm.), the stator must have a relatively long extension between its transmembrane domain and its PG-binding domain.

One of the important features of stator function is the mechanism by which it assembles into the motor. To produce a fully functional motor, multiple stator units have to be incorporated at appropriate positions around the rotor and anchored there to generate torque on the rotor. However, abrupt, stepwise drops and restorations of the rotation speed of the motor have been observed even in steadily rotating motors, suggesting that the stators are replaced frequently (Block and Berg, 1984; Blair and Berg, 1988; Sowa *et al*., 2005). In agreement with these observations, recent fluorescent photo-bleaching studies showed rapid exchange and turnover of the stator complexes in the functioning motor, revealing that the stator association to, and dissociation from, the PG layer is highly dynamic (Leake *et al*., 2006).

Overproduction of the MotA/MotB complex does not affect cell growth, suggesting that the proton-conducting activity of the MotA/MotB complex is tightly coupled to its incorporation around the rotor (Stolz and Berg, 1991). MotA/MotB complexes diffusing in the cytoplasmic membrane must have a mechanism to suppress proton flow through the channel that would otherwise harm the cell. Deletion of residues 53 though 66, just after its single transmembrane segment of MotB, causes proton leakage and arrests cell growth upon overproduction of the mutant MotB protein together with wild-type MotA (Hosking *et al*., 2006), suggesting that this 14-residue segment acts as a plug to suppress proton leakage until the MotA/MotB complex is properly installed into the motor.

Earlier studies demonstrated that a MotB mutant lacking residues 51–100 ($MotB_{\Delta L}$) can still form a stable, active stator and that a MotB mutant with an additional deletion of residues 271–309 is also functional, although unstable (Muramoto and Macnab, 1998). We therefore named the region containing residues 111–270 PEM (Periplasmic region Essential for Motility) (Fig. 1). The structure of PEM should provide essential information

about the molecular mechanisms of assembly, anchoring and activation of the stator. In this study, we determined the crystal structures of C-terminal fragments of MotB ($MotB_C$) that covers the entire PEM region. Based on the structure and subsequent structural-based mutational and biochemical studies, we propose a model for assembly coupled activation of the proton channel of the MotA/MotB complex.

Results and discussion

Structure determination

We recently showed that a C-terminal fragment of MotB consisting of residues 78–309 ($MotB_{C1}$; Fig. 1) forms dimer in the periplasm and inhibits the motility of wild-type cells, suggesting that $MotB_{C1}$ competes with the wild-type MotA/MotB complex for binding to stator attachment sites around the rotor (Kojima *et al.*, 2008a). Since ^{1}H-^{15}N Hetero-nuclear Single Quantum Coherence (HSQC) spectra indicate that $MotB_{C1}$ contains a highly mobile region composed of about 40 amino acid residues (data not shown), we constructed several N-terminally and/or C-terminally truncated $MotB_{C1}$ variants for crystallization (Fig. 1). We succeeded in crystallizing $MotB_{C2}$ (residues 99–276), $MotB_{C6}$ (residues 88–291) and $MotB_{C7}$ (residues 88–309) (Table S1). They were crystallized in three different space groups: Form I, $P3_221$ for $MotB_{C6}$ and $MotB_{C7}$; Form II, $C222_1$ for $MotB_{C2}$; and Form III, $P2_12_12_1$ for $MotB_{C2}$. We determined the structures of Form I from $MotB_{C6}$, Form II, and Form III at 2.0, 1.75 and 2.4 Å resolutions respectively (Table S1). We did not refine the structure of $MotB_{C7}$ because the portion on which we could have built an atomic model was the same as that of $MotB_{C6}$ (residues 108–282) and because the resolution was lower with $MotB_{C7}$. Since Form I contained one molecule, and Forms II and III both contained two molecules, in the asymmetric unit, we built and refined five atomic models. Each model had missing segments due to disorder (Table S2) except for one in Form II that resolved the entire chain of $MotB_{C2}$ (Fig. 2A). Since this model, refined at the highest resolution (1.75 Å), contains the largest number of residues (99–276) among the five models and covers PEM (111–270), and also because the other models adopt basically the same structure (Fig. 2B), we mainly describe the structure of $MotB_{C2}$ Form II.

Overall structure of $MotB_{C2}$

$MotB_{C2}$ appears as a single-domain structure with a long N-terminal α-helix (α1) protruding from the domain (Fig. 2). The core of the domain has a typical OmpA-like structure, which adopts a β-α-β-α-β-β fold, and shows considerable structural similarities to other PGB domains, such as the C-terminal regions of PAL (Parsons *et al.*, 2006), RmpM (Grizot and Buchanan, 2004) and MotY (Kojima *et al.*, 2008b) (Fig. S1). The long α1 helix is connected to PGB core structure through α2, which is perpendicular to α1, and strand β1, which is connected to β2

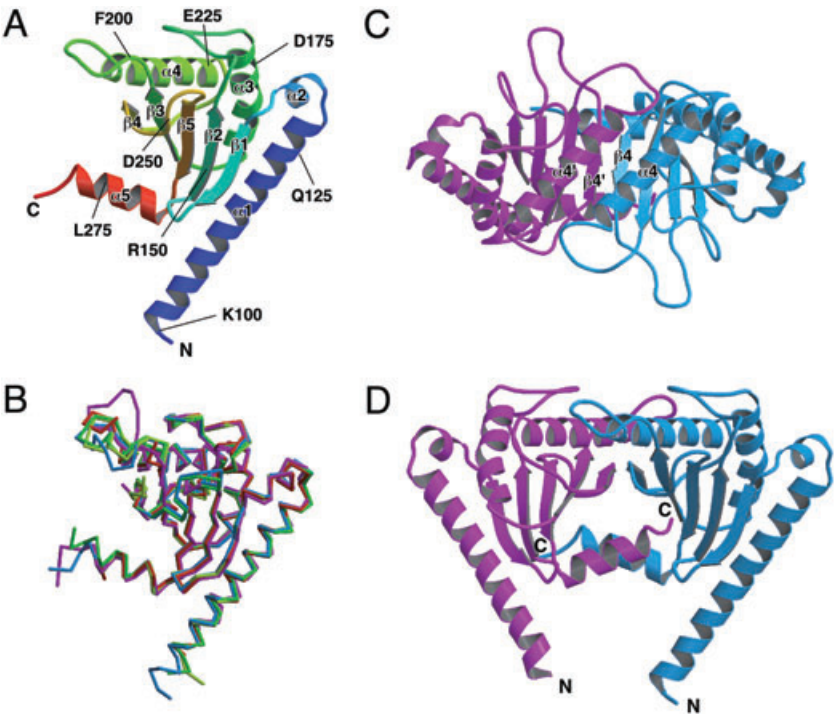

Fig. 2. Structure of the C-terminal fragment of MotB and its dimer.
A. Cα ribbon drawing of $MotB_{C2}$, colour coded from blue to red from the N- to the C-terminus. $MotB_{C2}$ contains the PGB core domain (α3, α4, β2, β3, β4 and β5) and N- and C-terminal substructures (α1, α2, α5 and β1).
B. Superposition of Cα traces of five independent structures in different crystal forms (magenta, Form I subunit A; cyan and green, Form II subunit A and B respectively; yellow and red, Form III subunit A and B respectively).
C and D. Cα ribbon representations of the $MotB_{C2}$ dimer along and perpendicular to the twofold axis. The two subunits are shown in cyan and magenta.

in the PGB core β-sheet and extends the sheet in an antiparallel manner. Although the N-terminal region of $MotB_{C2}$ shows a relatively low sequence similarity among MotB proteins from various bacterial species, secondary structures prediction by the PSIPRED server (Jones, 1999) suggests that α1, α2 and β1 are common structural elements (Fig. S2).

$MotB_{C2}$ forms a dimer through an interaction between its PGB domains (Fig. 2C and D). The subunit interface is composed of α4 and β4 (Fig. 2C). Strand β4 forms hydrogen bonds with its counterpart in an antiparallel manner (Figs 2C and 3A), producing a large, twisted intersubunit β-sheet. The two α4 helices also align antiparallel. The combined effect of these interactions is to make the two PGB domains tightly packed. These interactions, and the subunit arrangement for dimer formation, are totally different from those of *Helicobacter pylori* $MotB_C$ ($HpMotB_C$) (Roujeinikova, 2008) (Fig. S3), although the overall folds of the domain structures resemble each other.

Dimerization through the PGB domain is essential for proper arrangement of the proton channel

To examine the significance of dimer formation, we mutated residues of $MotB_{C6}$ on helix α4 at the dimer interface. Two of the changes introduce bulky side-chains that potentially disrupt the intersubunit interaction (A216W and D217W). The other two were substitutions that are known to impair motility (E213G and R223H) (Blair *et al.*, 1991; Togashi *et al.*, 1997) (Fig. 3A). $MotB_{C6}$ fragments with each of these substitutions were monomeric in solution, as determined by size-exclusion column chromatography (Fig. 3B). $MotB_{\Delta L}$ proteins with these replacements were coexpressed with MotA in an *E. coli* Δ*motAB* strain, and their motility was assayed on soft agar plates

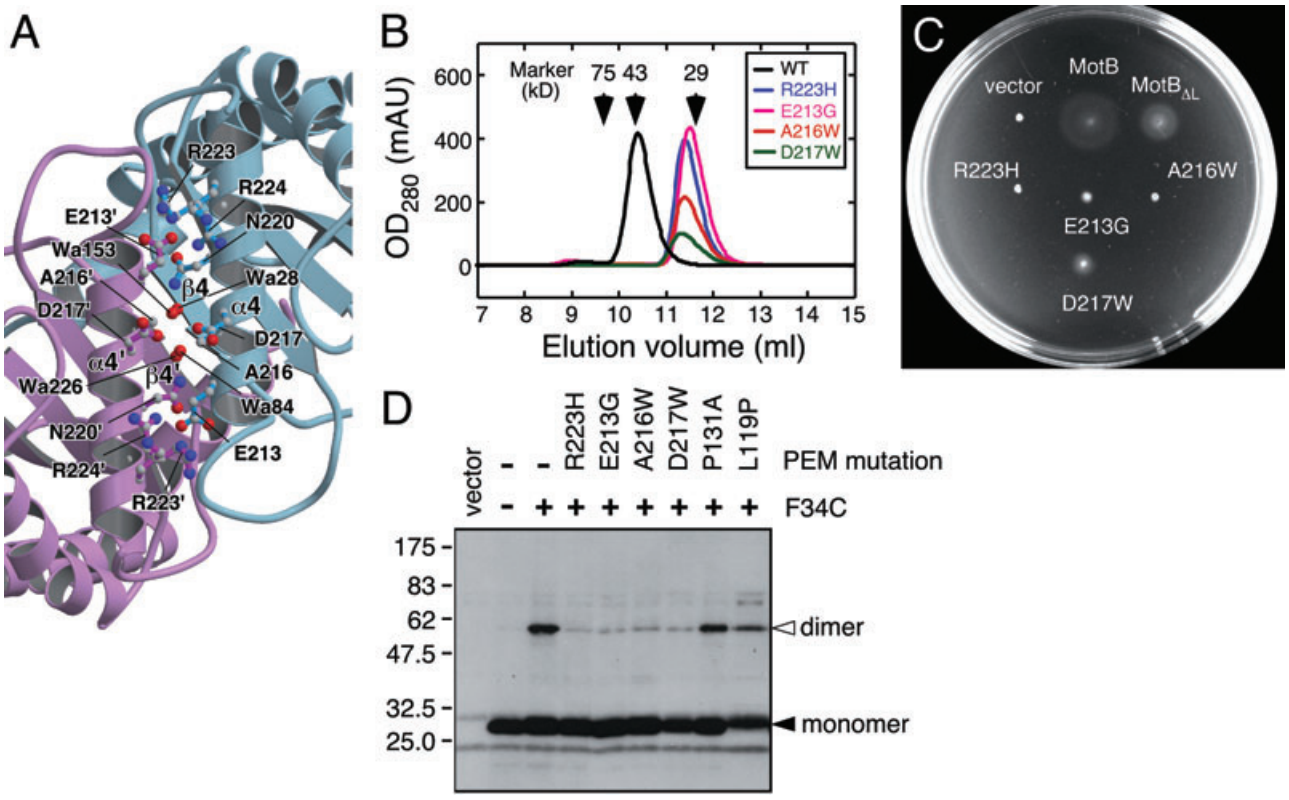

Fig. 3. $MotB_C$ dimer formation is crucial to functional stator formation.
A. Close-up view of the dimer interface. The two subunits are cyan and magenta respectively. Numbers labelled with a prime indicate the residues of the magenta subunit. Residues E213, D217, N220, R223 and R224 form a hydrophilic interaction network with water molecules. Side-chains of these residues are shown in a ball-and-stick representation with carbon atoms as small grey balls and nitrogen and oxygen atoms as large blue and red balls respectively.
B. Elution profile of purified $MotB_{C6}$ proteins by analytical size-exclusion chromatography.
C. Motility assay of Δ*motAB* cells containing plasmids encoding MotA and $MotB_{\Delta L}$ with or without mutations affecting the periplasmic dimer interface. The strain expressing MotA and full-length MotB was also assayed ('MotB'). The non-motile vector control is shown as 'pTrc99A' (RP6894 cells with pTrc99A).
D. Effect of mutations at the periplasmic dimer interface on disulphide cross-linking in the transmembrane segment of MotB. Note that the P131A substitution impairs neither motility nor disulphide cross-link formation. The cross-linked dimer was detected by immunobloting with anti-$MotB_C$ antibody.

(Fig. 3C). The mutations impaired motility either significantly or completely, suggesting that dimerization through the PGB domain is crucial to motor function.

How does disruption of dimerization of the PGB domains affect motility? Previous cross-linking studies demonstrated that the two transmembrane helices of the MotB dimer interact with each other in the $MotA_4/MotB_2$ complex (Braun and Blair, 2001; Braun *et al.*, 2004), raising the possibility that periplasmic dimer formation influences the arrangement of the transmembrane helices. Since the F34C substitution in the transmembrane helix of MotB can cross-link the MotB dimer in *E. coli* (Braun and Blair, 2001), we introduced this replacement into the four mutant $MotB_{\Delta L}$ proteins and coexpressed them with MotA in the *E. coli* Δ*motAB* strain. All the four proteins significantly reduced amounts of cross-linked dimer products (Fig. 3D), indicating that dimerization of the periplasmic region is required for the proper arrangement of the transmembrane helices that form the proton channel.

A large conformational change is required to anchor the MotA/MotB complex to the PG layer

Superposition of the structure of PAL bound to the PG precursor (PDB ID code 2aiz) (Parsons *et al.*, 2006) onto the $MotB_{C2}$ structure allowed us to predict the PGB site of $MotB_{C2}$ (Fig. 4A). It is located on the top surface of the $MotB_{C2}$ dimer opposite to α1. Most mutations that confer non- or slow-motile phenotypes (Blair *et al.*, 1991; Togashi *et al.*, 1997) target this putative PGB site (Fig. S1), an observation that supports the idea that this region is essential for anchoring the stator unit to the cell wall.

Since $MotB_{\Delta L}$ can form a functional stator with MotA, the $MotA/B_{\Delta L}$ complex must be anchored to the PG layer around the rotor. The α1 helices of the $MotB_{C2}$ dimer extend to the same side of the structure, and their N-termini are directly connected to the transmembrane dimer segments of $MotB_{\Delta L}$. This situation strongly suggests that the PGB dimer of $MotB_{\Delta L}$ stands on the cytoplasmic membrane surface with the two long α1 helices as its legs and the two α4 helices on the upper surface, where the PGB sites are located [Fig. 4B, (i)]. However, the $MotB_{C2}$ dimer is too small to reach the PG layer, since the distance between the surface of the hydrophobic core layer of the cytoplasmic membrane and that of the PG layer is about 100 Å, and the $MotB_{C2}$ dimer is only about 50 Å tall. For the PGB sites on the top surface of $MotB_{C2}$ to reach the PG layer, a large conformational change would be required. Because the PGB core forms a conserved, compact domain, the N-terminal region of PEM is not part of the PGB core. Thus, helices α1 and α2 and strand β1 are the most plausible candidates for being

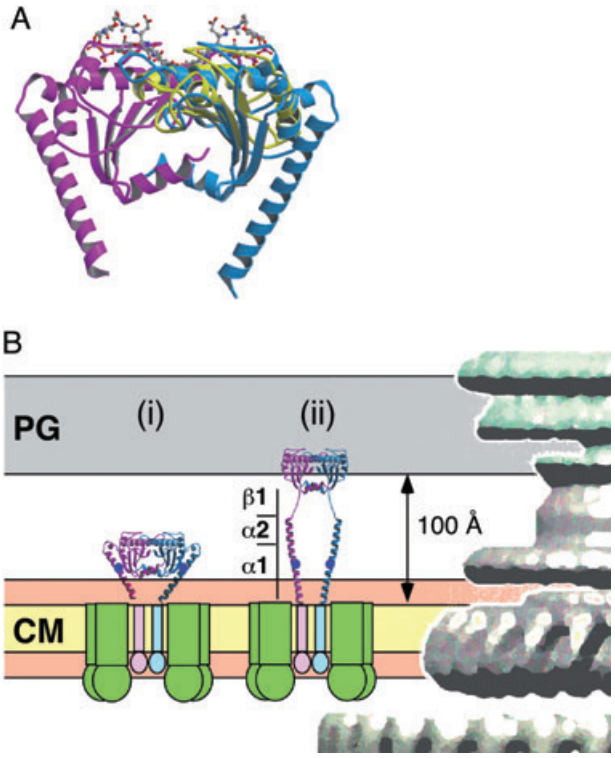

Fig. 4. Conformational changes of PEM required for anchoring the stator.
A. The possible PG binding site of $MotB_C$. The structure of *Haemophilus influenzae* Pal (yellow) complexed with a PG precursor (ball-and-stick) is superimposed on subunit A (cyan) and subunit B (magenta) of the $MotB_{C2}$ dimer. Note that only the PG precursor for the Pal complex superimposed on subunit B is shown.
B. Plausible models of $MotB_{\Delta L}$ in a freely diffusing, inactive form (i) and in a PG layer-anchored, active form assembled into the motor (ii). The cytoplasmic segments and the transmembrane helices of $MotB_{\Delta L}$ are displayed as rods and ellipsoids shown in pink and cyan. The green boxes and balls represent MotA subunits. Part of the flagellar basal body is shown on the right side. The hydrophilic surface and the hydrophobic core layers of the cytoplasmic membrane (CM) are shown in orange and yellow respectively. The relative sizes of $MotB_{\Delta L}$, the basal body, PG and CM are shown in the correct scale. The model in (i) is based on the crystal structure of the $MotB_{C2}$ dimer. The model in (ii) was constructed by changing several dihedral angles between α1 and α2, α2 and β1, and β1 and β2. Blue balls indicate the position of L119.

involved in the conformational change. If strand β1 detaches from the core β-sheet and extends colinearly with helices α1 and α2, the PGB domain would become long enough to reach the PG layer [Fig. 4B, (ii)].

The N-terminal region of PEM regulates proton translocation of the stator complex

We investigated the effects of several residue substitutions in the N-terminal region of PEM and found that L119P and L119E in α1 (Fig. 5A) affected cell growth without impairing motility (Fig. 5B). When $MotB_{\Delta L}$ mutants

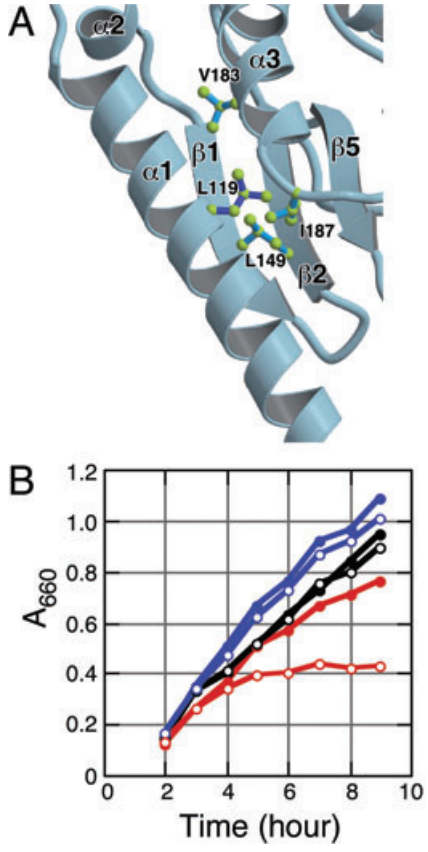

Fig. 5. Effect of amino acid substitutions at Leu-119 of MotB.
A. The structure of $MotB_{C2}$ in the vicinity of L119. Residue L119 and residues contacting L119 are shown in ball-and-stick representations, with L119 highlighted in blue.
B. Effect of the L119P mutation on cell growth. Growth was measured for Δ*motAB* cells containing plasmid pTSK30 encoding full-length MotA and $MotB_{\Delta L}$ with or without the L119P substitution. Cells with full-length MotA and MotB (expressed from plasmid pNSK9) were also examined. The black line shows full-length MotB; the blue line shows $MotB_{\Delta L}$; red line shows $MotB_{\Delta L}$(L119P). Open and filled circles indicate IPTG-induced and non-induced cells respectively.

with either of these two changes were co-overexpressed with MotA in the Δ*motAB* strain, motility was normal but growth was severely impaired. In contrast, no significant growth impairment was observed with full-length MotB and $MotB_{\Delta L}$ or with $MotB_{\Delta L}$(L119P/E) without induction by IPTG (Fig. 5B). Cells expressing $MotA/B_{\Delta L}$(L119P/E) formed chemotactic rings significantly larger than those formed by cells expressing $MotA/B_{\Delta L}$ under non-inducing condition (Fig. S4) and swam vigorously under an optical microscope, suggesting that the conformation of the $MotA/B_{\Delta L}$(L119P/E) complex is more favourable than that of $MotA/B_{\Delta L}$ for efficient assembly into the motor. The L119P substitution does not seem to affect the arrangement of the transmembrane helices of the MotB dimer, based on the extent of disulphide cross-linking (Fig. 3D). Thus, the two changes at L119 must alter the conformation of the $MotA/B_{\Delta L}$ complex to allow proton translocation so that a massive proton influx causes growth impairment (Hosking *et al.*, 2006).

A region from P52 to P65 just after the transmembrane segment of *E. coli* MotB (P53 to P66 in *Salmonella* MotB) has been proposed as a 'plug' for the proton channel when the MotA/B complex is not assembled (Hosking *et al.*, 2006). Deletion of this plug region inhibits cell growth, but not motility, by acidifying the cytoplasm, suggesting that the plug regulates proton translocation depending on the assembly state of the stator. However, expression of $MotB_{\Delta L}$, although it lacks the plug region, does not impair growth, indicating that some other region within PEM can also plug the proton channel. It could be that the whole of $MotB_{C2}$ plugs the channel, as depicted in Fig. 4B, or that a specific arrangement of the transmembrane helices suppresses proton translocation because of the way it is attached to the $MotB_{C2}$ dimer. The L119P/E mutations in helix α1 must destabilize the hydrophobic interactions with L149 in strand β2 and V183 and I187 after helix α3 (Fig. 5A). The loss of interactions of α1, α2 and β1 with the PGB core may allow $MotB_{\Delta L}$ to take an extended conformation (Fig. 4B) and to open the proton channel even when the $MotA/B_{\Delta L}$ complex is not assembled into the motor. The detachment of a strand from a β-sheet may appear rather drastic and unlikely. However, β1, α1 and α2 are not fully involved in the hydrophobic core of the PGB core domain, and such conformational changes involving peripheral elements have been observed in intermolecular β-sheets of many other protein complexes (Shin *et al.*, 2003; Ranson *et al.*, 2006).

Model for activation of the proton channel by association with the stator

Based on the structure of $MotB_{C2}$ and the biochemical analyses described above, we propose that the activation of the proton channel of the MotA/B complex is coupled to the anchoring of the complex around the rotor. Initially, the MotA/B complex would diffuse through the cytoplasmic membrane. Even with the addition of the 60-residue linker to the transmembrane segment and the 37-residue C-terminal region, which are not present in $MotB_{C2}$, the periplasmic domain would probably not contact the PG layer. When the MotA/B complex encounters a rotor, interactions between the cytoplasmic domain of MotA and FliG in the C-ring (Zhou *et al.*, 1998a) could trigger conformational changes in the N-terminal region of PEM that open the proton channel and allow the PGB domain to anchor to the PG layer. Although this general type of mechanism has been proposed previously (Van Way *et al.*, 2000; Hosking *et al.*, 2006), our study reveals a possible structural basis for the conformational changes. Further

studies, such as testing the effect of cross-linking the long α1 helix to the PGB core or the crystal structure analysis of a $MotB_C$ fragment with the L119P/E substitutions, which are currently underway, will be required to determine whether these events actually occur within the cell envelope.

Experimental procedures

Bacterial strains, plasmids and mutagenesis

Bacterial strains and plasmids used in this study are listed in Table S3. The plasmid containing in-frame deletion of MotB (pTSK30) was constructed as described by Toker *et al.* (1996). All the mutations in MotB were generated by the QuikChange site-directed mutagenesis method, as described previously (Kojima *et al.*, 2008a). For the functional and cross-linking assays for each MotB mutant, we mutated *motB*(Δ51–100) in the plasmid pTSK30, and for the biochemical assays with the mutant $MotB_{C6}$ fragment, mutations were introduced into the plasmid pTSK17.

Protein expression and purification

The genes encoding *Salmonella typhimurium* MotB residues 99–276 ($MotB_{C2}$), 88–291 ($MotB_{C6}$) and 88–309 ($MotB_{C7}$) were PCR-cloned into the vector pET19b (Novagen) and overexpressed with a 5-histidine (for $MotB_{C2}$) or 6-histidine (for $MotB_{C6}$ and $MotB_{C7}$) tag in *E. coli* strain BL21(DE3), as described previously (Kojima *et al.*, 2008a). For overexpression of $MotB_{C6}$ labelled with Se-Met (Se-Met $MotB_{C6}$), we used B834(DE3) cells carrying the pLysS plasmid as the expression host. Cells were collected by centrifugation and suspended in buffer A (20 mM Tris-HCl pH 8.0, 150 mM NaCl) containing one tablet of Complete Protease Inhibitor cocktail (Roche Diagnostics). Cells were disrupted by French Press (Ohtake Works) and lysates were centrifuged at 100 000 *g* for 30 min. The soluble fraction was loaded onto a HisTrap column (GE Healthcare). His-tagged $MotB_C$ fragments were eluted by a linear 0–500 mM gradient of imidazole in buffer A. $MotB_{C2}$ and $MotB_{C7}$ were pure enough for crystallization after the HisTrap column. $MotB_{C6}$ was further purified using a HiTrapQ column (GE Healthcare) with a linear gradient of 10–1000 mM NaCl in buffer B (20 mM Tris-HCl pH 8.0, 10 mM NaCl). Peak fractions were pooled and concentrated in buffer C (20 mM Tris-HCl pH 8.0, 100 mM NaCl) by ultrafiltration using an Amicon Ultra device (Millipore). Final concentrations of purified $MotB_C$ fragments used for crystallization were: 57 mg ml^{-1} ($MotB_{C6}$), 18 mg ml^{-1} ($MotB_{C2}$), 32 mg ml^{-1} ($MotB_{C7}$) and 60 mg ml^{-1} (Se-Met $MotB_{C6}$). Se-Met $MotB_{C6}$ was purified by the same procedure as described $MotB_{C6}$.

Crystallization, data collection and structure determination

Crystals were obtained at 20°C using the sitting-drop vapour-diffusion method by mixing a 1 μl protein solution with a 1 μl reservoir solution. The protein fragments were crystallized into various forms under various conditions (Table S1). Crystals were soaked in a solution containing 90% (v/v) of the reservoir solution and 10% (v/v) MPD for a few seconds, and then immediately transferred into liquid nitrogen for freezing. All the X-ray diffraction data were collected under helium gas flow at −233°C using a synchrotron beamline BL41XU of SPring-8 (Harima, Japan). The data were processed with MOSFLM (Leslie, 1992) and scaled with SCALA (Collaborative Computational Project Number 4, 1994). Phase calculation was performed with SOLVE (Terwilliger and Berendzen, 1999) using the anomalous diffraction data from the Form I crystal of Se-Met $MotB_{C6}$. The best electron-density map was obtained from MAD phases followed by density modification with DM (Collaborative Computational Project Number 4, 1994). The model was constructed with COOT (Emsley and Cowtan, 2004) and was refined against the Se-Met $MotB_{C6}$ data to 2.0 Å using program CNS (Brunger *et al.*, 1998). A 5% fraction was excluded from the data for the R-free calculation. During the refinement process, iterative manual modifications were performed using 'omit map'. Structures of the Form II crystal of $MotB_{C2}$ and the Form III crystal of $MotB_{C6}$ were determined by molecular replacement using MOLREP (Collaborative Computational Project Number 4, 1994). Data collection and refinement statistics are summarized in Tables S2 and S4.

The atomic co-ordinates and structure factors of $MotB_{C6}$ Form I, $MotB_{C2}$ Form II and $MotB_{C2}$ Form III have been deposited with the accession codes 2zov, 2zvy and 2zvz respectively.

Analytical size-exclusion column chromatography

Analytical size-exclusion chromatography of purified $MotB_{C6}$ fragments was performed with a Superdex 75 10/300 GL column (GE Healthcare), as described previously (Kojima *et al.*, 2008a).

Motility assay

We used the *E. coli* Δ*motAB* strain RP6894 as the host to assess functional properties of mutant MotB proteins. RP6894 cells harbouring plasmid pTSK30 encoding *motA* and *motB*(Δ51–100) with or without *motB* mutations were grown overnight at 30°C in tryptone broth [1% (w/v) tryptone, 0.5% NaCl] containing 100 μg ml^{-1} ampicillin. A 1 μl aliquot of an overnight culture was spotted on a tryptone soft-agar plate containing ampicillin and 0.1 mM IPTG and incubated at 30°C for 8 h.

Growth curves

Growth was monitored as described (Zhou *et al.*, 1998b). RP6894 cells harbouring respective plasmids were grown overnight at 30°C in tryptone broth containing 100 μg ml^{-1} ampicillin. The culture was then diluted 1:30 in 3 ml of the same medium and shaken at 30°C. IPTG was added to a final concentration of 0.1 mM after 3 h and A_{660} was measured every hour.

Oxidative cross-linking

Cross-linking experiments were performed on whole cells of strain RP6894 harbouring pTSK30 plasmids encoding *motA* and *motB*(Δ51–100) with or without *motB* mutations, following the method described previously (Braun *et al.*, 2004). Cells were grown at 30°C to log phase in tryptone broth containing 100 μg ml^{-1} ampicillin and 0.1 mM IPTG, harvested by centrifugation, re-suspended in 50 mM Tris-HCl, pH 8.0, containing 20 mM EDTA to an OD_{660} of 5.0. Disulphide cross-linking was induced with 100 μM iodine for 2 min at room temperature and then quenched with 10 mM NEM. Cross-linked products were analysed by SDS-PAGE under non-reducing conditions, followed by immunoblotting with polyclonal anti-$MotB_C$ antibody.

Acknowledgements

We thank T. Kato and K. Iwasaki for invaluable discussions, S. Tatematsu for technical assistance, N. Shimizu, M. Kawamoto, K. Hasegawa and M. Yamamoto at SPring-8 for technical help in use of beamlines. This work was supported in part by Grants-in-Aid for Scientific Research [to S.K. (18054010), K.I. (18074006), H.M. (18074003) and K.N. (16087207)] from the Ministry of Education, Science and Culture of Japan.

References

Berg, H.C. (2003) The rotary motor of bacterial flagella. *Annu Rev Biochem* **72:** 19–54.

Blair, D.F., and Berg, H.C. (1988) Restoration of torque in defective flagellar motors. *Science* **242:** 1678–1681.

Blair, D.F., and Berg, H.C. (1990) The MotA protein of *E. coli* is a proton-conducting component of the flagellar motor. *Cell* **60:** 439–449.

Blair, D.F., Kim, D.Y., and Berg, H.C. (1991) Mutant MotB proteins in *Escherichia coli*. *J Bacteriol* **173:** 4049–4055.

Block, S.M., and Berg, H.C. (1984) Successive incorporation of force-generating units in the bacterial rotary motor. *Nature* **309:** 470–472.

Braun, T.F., and Blair, D.F. (2001) Targeted disulfide cross-linking of the MotB protein of *Escherichia coli*: evidence for two H^+ channels in the stator complex. *Biochemistry* **40:** 13051–13059.

Braun, T.F., Al-Mawsawi, L.Q., Kojima, S., and Blair, D.F. (2004) Arrangement of core membrane segments in the MotA/MotB proton-channel complex of *Escherichia coli*. *Biochemistry* **43:** 35–45.

Brunger, A.T., Adams, P.D., Clore, G.M., DeLano, W.L., Gros, P., Grosse-Kunstleve, R.W., *et al.* (1998) Crystallography and NMR system: a new software suite for macromolecular structure determination. *Acta Crystallogr D Biol Crystallogr* **54:** 905–921.

Che, Y.S., Nakamura, S., Kojima, S., Kami-ike, N., Namba, K., and Minamino, T. (2008) Suppressor analysis of the MotB (D33E) mutation to probe bacterial flagellar motor dynamics coupled with proton translocation. *J Bacteriol* **190:** 6660–6667.

Chun, S.Y., and Parkinson, J.S. (1988) Bacterial motility: membrane topology of the *Escherichia coli* MotB protein. *Science* **239:** 276–278.

Collaborative Computational Project Number 4 (1994) The CCP4 suite: programs for protein crystallography. *Acta Crystallogr D Biol Crystallogr* **50:** 760–763.

De Mot, R., and Vanderleyden, J. (1994) The C-terminal sequence conservation between OmpA-related outer membrane proteins and MotB suggests a common function in both gram-positive and gram-negative bacteria, possibly in the interaction of these domains with peptidoglycan. *Mol Microbiol* **12:** 333–334.

Emsley, P., and Cowtan, K. (2004) Coot: model-building tools for molecular graphics. *Acta Crystallogr D Biol Crystallogr* **60:** 2126–2132.

Grizot, S., and Buchanan, S.K. (2004) Structure of the OmpA-like domain of RmpM from *Neisseria meningitidis*. *Mol Microbiol* **51:** 1027–1037.

Hirota, N., and Imae, Y. (1983) Na^+-driven flagellar motors of an alkalophilic *Bacillus* strain YN-1. *J Biol Chem* **258:** 10577–10581.

Hosking, E.R., Vogt, C., Bakker, E.P., and Manson, M.D. (2006) The *Escherichia coli* MotAB proton channel unplugged. *J Mol Biol* **364:** 921–937.

Jones, D.T. (1999) Protein secondary structure prediction based on position-specific scoring matrices. *J Mol Biol* **292:** 195–202.

Kojima, S., Furukawa, Y., Matsunami, H., Minamino, T., and Namba, K. (2008a) Characterization of the periplasmic domain of MotB and implications for its role in the stator assembly of the bacterial flagellar motor. *J Bacteriol* **190:** 3314–3322.

Kojima, S., Shinohara, A., Terashima, H., Yakushi, T., Sakuma, M., Homma, M., *et al.* (2008b) Insights into the stator assembly of the *Vibrio* flagellar motor from the crystal structure of MotY. *Proc Natl Acad Sci USA* **105:** 7696–7701.

Leake, M.C., Chandler, J.H., Wadhams, G.H., Bai, F., Berry, R.M., and Armitage, J.P. (2006) Stoichiometry and turnover in single, functioning membrane protein complexes. *Nature* **443:** 355–358.

Leslie, A.G.W. (1992) CCP4+ESF-EACMB. *Newsl Protein Crystallogr* **26:** 27–33.

Manson, M.D., Tedesco, P., Berg, H.C., Harold, F.M., and van der Drift, C. (1977) A protonmotive force drives bacterial flagella. *Proc Natl Acad Sci USA* **74:** 3060–3064.

Matias, V.R.F., Al-Amoudi, A., Dubochet, J., and Beveridge, T.J. (2003) Cryo-transmission electron microscopy of frozen-hydrated sections of *Escherichia coli* and *Pseudomonas aeruginosa*. *J Bacteriol* **185:** 6112–6118.

Matsuura, S., Shioi, J., and Imae, Y. (1977) Motility in *Bacillus subtilis* driven by an artificial protonmotive force. *FEBS Lett* **82:** 187–190.

Minamino, T., Imada, K., and Namba, K. (2008) Molecular motors of the bacterial flagella. *Curr Opin Struct Biol* **18:** 693–701.

Muramoto, K., and Macnab, R.M. (1998) Deletion analysis of MotA and MotB, components of the force-generating unit in the flagellar motor of *Salmonella*. *Mol Microbiol* **29:** 1191–1202.

Parsons, L.M., Lin, F., and Orban, J. (2006) Peptidoglycan

recognition by Pal, an outer membrane lipoprotein. *Biochemistry* **45:** 2122–2128.
Ranson, N.A., Clare, D.K., Farr, G.W., Houldershaw, D., Horwich, A.L., and Saibil, H.R. (2006) Allosteric signaling of ATP hydrolysis in GroEL–GroES complexes. *Nat Struct Mol Biol* **13:** 147–152.
Reid, S.W., Leake, M.C., Chandler, J.H., Lo, C.J., Armitage, J.P., and Berry, R.M. (2006) The maximum number of torque-generating units in the flagellar motor of *Escherichia coli* is at least 11. *Proc Natl Acad Sci USA* **103:** 8066–8071.
Roujeinikova, A. (2008) Crystal structure of the cell wall anchor domain of MotB, a stator component of the bacterial flagellar motor: implications for peptidoglycan recognition. *Proc Natl Acad Sci USA* **105:** 10348–10353.
Shin, D.S., Pellegrini, L., Daniels, D.S., Yelent, L.C., Bates, D., Yu, D.S., *et al.* (2003) Full-length archaeal Rad51 structure and mutants: mechanisms for RAD51 assembly and control by BRCA2. *EMBO J* **22:** 4566–4576.
Sowa, Y., and Berry, R.M. (2008) Bacterial flagellar motor. *Q Rev Biophys* **41:** 103–132.
Sowa, Y., Rowe, A.D., Leake, M.C., Yakushi, T., Homma, M., Ishijima, A., *et al.* (2005) Direct observation of steps in rotation of the bacterial flagellar motor. *Nature* **437:** 916–919.
Stolz, B., and Berg, H.C. (1991) Evidence for interactions between MotA and MotB, torque-generating elements of the flagellar motor of *Escherichia coli*. *J Bacteriol* **173:** 7033–7037.
Terashima, H., Kojima, S., and Homma, M. (2008) Flagellar motility in bacteria structure and function of flagellar motor. *Int Rev Cell Mol Biol* **270:** 39–85.
Terwilliger, T.C., and Berendzen, J. (1999) Automated MAD and MIR structure solution. *Acta Crystallogr D Biol Crystallogr* **55:** 849–861.
Togashi, F., Yamaguchi, S., Kihara, M., Aizawa, S.I., and Macnab, R.M. (1997) An extreme clockwise switch bias mutation in *fliG* of *Salmonella typhimurium* and its suppression by slow-motile mutations in *motA* and *motB*. *J Bacteriol* **179:** 2994–3003.
Toker, A.S., Kihara, M., and Macnab, R.M. (1996) Deletion analysis of the FliM flagellar switch protein of *Salmonella typhimurium*. *J Bacteriol* **178:** 7069–7079.
Van Way, S.M., Hosking, E.R., Braun, T.F., and Manson, M.D. (2000) Mot protein assembly into the bacterial flagellum: a model based on mutational analysis of the *motB* gene. *J Mol Biol* **297:** 7–24.
Zhou, J., Lloyd, S.A., and Blair, D.F. (1998a) Electrostatic interactions between rotor and stator in the bacterial flagellar motor. *Proc Natl Acad Sci USA* **95:** 6436–6441.
Zhou, J., Sharp, L.L., Tang, H.L., Lloyd, S.A., Billings, S., Braun, T.F., and Blair, D.F. (1998b) Function of protonatable residues in the flagellar motor of *Escherichia coli*: a critical role for Asp 32 of MotB. *J Bacteriol* **180:** 2729–2735.

Supporting information

Additional supporting information may be found in the online version of this article.

Please note: Wiley-Blackwell are not responsible for the content or functionality of any supporting materials supplied by the authors. Any queries (other than missing material) should be directed to the corresponding author for the article.

